Appendices

Appendix A Microclimate and background weather conditions during survey

Table A1 Microclimate conditions during survey and background weather conditions

Date	Strat time	Microclimate condition during measurement [1]											Weather condition of the day [3]				
		Ta (°C)			Rh (%)			Tmrt (°C)			*v*_mean (m/s)	VHD warning [2]	Ta (°C)			Rh_mean (%)	Cloud_mean (%)
		Mean	Min	Max	Mean	Min	Max	Mean	Min	Max			Max	Min	Mean		
07/07	11:25	32.54	31.53	33.27	75.10	73.14	78.03	42.71	39.97	45.17	1.20	√	33.4	29.0	30.4	76	71
07/08	11:14	32.75	31.77	34.14	73.25	67.85	76.36	44.34	31.37	61.73	1.09	√	33.2	28.8	30.4	76	48
07/14	11:28	34.54	33.51	35.82	59.55	55.24	62.95	46.72	32.56	65.64	1.22	√	33.8	28.5	31.3	71	68
07/28	15:13	35.30	34.71	36.86	57.40	52.25	60.46	43.10	35.03	74.07	1.20	√	34.7	28.9	31.5	72	86
07/28	15:48	35.35	34.65	36.78	57.22	53.37	61.34	41.15	33.86	56.72	0.94	√					
07/31	9:44	31.95	31.36	32.80	74.59	70.38	77.88	45.22	32.42	62.07	0.99		32.5	26.5	29.1	84	85
07/31	10:30	32.06	31.52	33.34	72.41	66.60	76.83	42.61	30.57	59.96	0.96						
08/02	10:23	33.23	32.84	34.20	57.88	52.87	61.13	45.09	30.19	64.32	0.97	√	34.6	27.9	30.4	70	52
08/02	10:54	33.45	32.72	34.42	55.11	51.11	58.58	40.06	32.14	63.39	1.10	√					
08/02	11:35	34.09	33.09	35.01	51.54	47.43	53.76	45.74	32.49	59.68	1.51	√					
08/03	10:28	33.15	32.32	34.34	61.01	57.64	63.23	45.42	31.72	62.36	1.18	√	35.1	27.9	30.8	73	43
08/05	13:20	33.93	32.79	34.98	70.94	66.61	74.65	45.94	31.68	70.16	0.81	√	33.0	28.3	30.4	79	84
08/05	14:26	32.67	31.93	33.24	73.21	69.98	77.91	41.26	33.19	59.73	1.96	√					
08/05	14:59	33.37	32.82	33.95	71.36	68.45	74.31	41.38	32.21	53.10	1.08	√					
08/05	16:09	32.80	31.96	33.28	72.33	70.93	74.62	41.11	30.59	65.91	2.17	√					
08/05	16:38	32.99	32.39	33.40	71.35	69.71	72.91	41.70	31.57	62.94	1.68	√					
08/08	11:41	33.68	32.25	34.64	68.26	64.41	70.94	48.57	34.73	73.85	1.40	√	33.3	28.9	30.3	74	69
08/09	15:25	32.83	32.08	34.10	76.60	70.66	79.60	39.36	32.68	62.55	1.05	√	32.8	28.7	30.3	76	73
08/09	15:56	32.42	31.64	32.96	78.02	75.52	80.16	42.16	32.06	61.96	1.27	√					

08/12	14:18	32.58	31.73	33.36	69.04	66.18	72.12	48.22	32.30	70.15	1.86						
08/12	14:53	31.89	31.47	32.23	73.24	72.16	75.85	39.57	31.51	59.95	1.20		32.1	26.6	29.0	79	86
08/12	15:50	31.08	30.57	31.44	76.38	73.43	77.87	34.65	30.91	42.04	0.97						
08/15	14:42	32.10	30.78	33.66	75.95	71.22	79.36	38.83	30.54	72.74	1.28						
08/15	15:52	30.58	29.56	31.69	81.04	74.33	90.27	34.61	29.84	42.67	0.62		32.5	28.8	29.9	80	85
08/15	16:23	31.07	30.82	31.37	78.65	76.77	81.39	34.15	30.08	43.87	0.77						
08/16	14:30	34.22	33.41	35.99	69.90	65.46	72.83	49.31	34.70	68.90	0.98	√					
08/16	15:41	33.99	33.05	35.43	66.26	62.81	69.74	45.39	32.06	64.31	0.83	√	34.0	28.8	30.6	78	70
08/16	16:06	33.09	32.74	33.71	68.78	65.45	71.73	37.51	32.04	57.74	0.77	√					
08/20	14:34	31.08	30.27	32.07	75.94	70.04	84.84	36.70	30.38	44.17	0.74		31.5	28.4	29.7	80	86
08/20	15:07	31.12	30.70	31.42	76.61	74.12	83.15	34.12	29.83	38.98	0.35						
08/21	14:50	31.06	30.71	31.25	79.40	76.70	86.85	33.78	30.46	38.57	0.76						
08/21	15:51	31.14	30.76	31.48	78.65	75.83	82.86	35.35	31.06	46.49	0.62		32.1	28.2	29.6	82	86
08/21	16:16	30.93	30.76	31.20	77.48	75.83	79.05	32.10	30.48	34.54	0.79						
08/22	11:39	30.67	29.97	32.39	82.03	76.51	84.56	39.63	29.38	60.04	0.63						
08/22	12:30	32.81	31.57	33.97	71.61	67.59	74.55	50.15	35.83	58.78	0.94						
08/22	12:58	32.36	31.85	32.86	71.51	69.31	74.00	36.08	31.97	48.65	1.00		33.0	28.0	30.0	79	88
08/22	14:42	32.79	32.00	33.55	71.78	69.54	74.02	43.61	30.34	58.72	1.06						
08/22	15:11	32.71	32.19	33.52	71.50	69.71	73.72	46.29	31.22	60.18	0.94	√					
08/26	10:39	30.33	29.37	30.95	82.89	77.46	88.83	33.56	28.32	37.06	0.40		32.8	27.9	29.7	83	88
09/04	14:35	33.68	33.01	34.31	65.91	63.94	68.83	41.13	33.27	52.87	0.93	√	32.6	27.3	29.9	73	87
09/04	15:07	33.17	32.63	34.02	67.58	64.77	70.48	33.41	30.85	35.88	0.53	√					
09/13	13:13	29.52	28.90	30.17	84.80	81.33	89.34	36.91	28.65	53.92	0.92		30.4	26.8	27.9	88	87
09/13	13:41	28.90	28.57	29.25	86.02	84.89	87.64	31.83	28.15	37.47	1.52						
09/17	14:35	31.07	29.85	32.30	77.54	73.21	81.23	40.13	29.47	59.28	1.51		31.7	26.8	28.5	85	79
09/19	11:13	32.07	31.30	33.34	67.43	62.61	70.62	36.86	29.99	55.43	0.68		33.5	27.3	29.5	79	48
09/20	9:18	30.06	29.70	30.52	80.26	76.98	82.72	33.03	29.41	38.51	1.02	√	32.9	27.5	29.6	76	28
09/20	10:31	30.92	30.03	32.01	76.41	72.20	79.82	38.90	29.21	63.08	1.21	√					

09/20	14:44	31.90	30.68	33.06	73.10	66.03	82.13	40.99	30.09	64.34	0.69	√					
09/20	15:18	32.13	31.71	32.92	68.12	65.30	70.89	39.85	30.42	59.24	0.76	√					
09/21	10:46	31.25	30.94	31.79	78.25	75.75	80.34	34.32	30.09	49.91	0.61	√					
09/21	11:43	32.93	32.16	34.34	72.67	67.35	74.68	45.09	31.61	60.69	1.47	√	33.6	27.6	30.0	77	28
09/21	12:30	33.80	33.00	34.64	69.15	64.71	71.58	51.28	31.58	67.51	1.69	√					
09/22	15:08	32.72	32.06	33.77	66.95	63.94	69.97	38.87	31.34	52.19	1.35	√	34.4	28.4	30.2	75	67
09/22	15:36	31.64	31.28	32.16	68.90	66.84	72.23	32.24	30.85	33.56	0.96	√					
09/23	12:08	32.33	31.57	33.24	65.35	62.33	67.01	38.95	30.72	64.18	1.28	√					
09/23	15:10	32.59	31.72	33.29	63.93	61.47	66.50	35.17	30.24	41.29	1.04	√	33.7	28.3	30.1	74	52
09/23	16:51	30.62	30.45	30.86	72.31	71.27	73.65	31.32	30.00	33.21	1.08	√					

1 Calculated by using the data collected at all stopping points. For the calculation of Tmrt, refer to the method section.

2 *VHD* very hot days warning. Data from Hong Kong Observatory.

3 Data collected from Hong Kong Observatory.

Appendix B Microclimate measurement and data preprocessing details

B.1 Microclimate measurement instrument

Fig. B1 shows the backpack station we used to conduct mobile measurement of thermal exposure along with the participant, which was equipped with the devices introduced in Table 1. Ta, Rh, and *v* were measured with Testo 480 and calibrated sensors. They feature exposed sensors, which enable fast reaction time under walking condition. Two black globes were used to measure Tg, i.e., one 40mm black globe made from a table-tennis ball painted with black matt paint, and one 25.4mm copper black globe on Kestrel 5400 Heat Stress Tracker. The 25.4mm copper black globe on Kestrel 5400 Heat Stress Tracker requires 8min to reach 95% accuracy after dramatic environmental changes, according to the user manual. Although less accurate compared to a metallic black globe due to the thermal property of plastic [1], black globes made from table-tennis balls feature dramatically shorter response time, reported as short as several minutes [2,3], which is more appropriate for measurement during walking. Comparatively, the three Apogee net radiometers used to measure longwave and shortwave radiation in six directions feature a responding time of 1s, and can therefore well depict the radiation condition along the route without lag.

Fig. B1 Backpack microclimate measurement instrument

Among these devices, Kestrel 5400 measures Tg with a 25.4mm copper black globe. As introduced by the instrument supplier, it approximates standard Tg by using the ASHRAE's Tmrt Equivalent method,

$$T_{mrt} = \left[\left(T_g + 273.15\right)^4 + \frac{1.10 \times 10^8 \times v^{0.6} \times (T_g - T_a)}{\varepsilon \times d^{0.4}} \right]^{0.25} \tag{B0}$$

where T_g is globe temperature, T_a is air temperature, v is wind velocity, d is the globe diameter, and ε is the emissivity of the black globe.

Therefore, the output T_g of Kestrel 5400, which is converted to standard black globe, is influenced by the *v* measured by itself, and by not using Kestrel to measure *v*, more accurate T_g could be obtained. We therefore didn't measure *v* with Kestrel 5400.

In addition, to match the data sampling frequency of other devices, the measured Tg were interpolated by using the mean of adjacent two measured values. The interpolated values were only used in the cross correlation analyses.

B.2 Details of thermal comfort and heat stress indices calculation

B.2.1 Calculation of PET and mPET

We calculated PET and mPET by using Biometeo 0.2.9 [4], which can perform more accurate calculation compared to Rayman. Table B1 demonstrates the input parameters for the calculation of PET and mPET. Default settings for personal data were applied, while inputs of clothing and activity were accommodated. For PET calculation, default clothing and activity level is used, so that the results can be compared with the past local benchmarks which have used the same settings. Yet for mPET, the metabolic rate 165W/m^2 for walking on ground level at a speed of 4km/h, and thermal insulation 0.5clo for summertime daily wearing (with underpants, shirt with short sleeves, light trousers, light socks, and shoes) were used [5], which are consistent with the situation of the walking survey.

Table B1 Input parameters for calculation of PET and mPET

Category	Item	PET calculation	mPET calculation
Personal data	Height (m)	1.75	
	Weight (kg)	75.0	
	Age (a)	35	
	Gender	Male	
Clothing and activity	Clothing (clo)	0.9	0.5
	Activity (W)	80	165
	Position	Standing	

B.2.2 Natural web bulb temperature estimation method

To calculate HKHI by using formula (3), natural web bulb temperature (T_{nw}) is required as an input parameter. We spotted two ways of estimating T_{nw} with the microclimate variables we measured, i.e., Ta, Rh, *v*, and Tmrt.

The first is a set of empirical models summarized by Bernard [6]. This estimation method is also adopted by Kestrel instruments, as introduced by Carter et al. [7]. This method estimates T_{nw} from psychrometric wet bulb temperature (T_{pwb}), and considers low and high radiant heat conditions, as shown in formula (B1).

$$T_{nw} = \begin{cases} T_a - C \times \left(T_a - T_{pwb}\right), \ if \ T_{g150} - T_a < 4 \\ T_{pwb} + 0.25\left(T_{g150} - T_a\right) + e, \ if \ T_{g150} - T_a \geq 4 \end{cases} \tag{B1}$$

where $C = \begin{cases} 0.85 & , v < 0.03 \\ 0.96 + 0.069 \log_{10} v & , 0.03 \leq v \leq 3 \\ 1.0 & , v > 3 \end{cases}$, and $e = \begin{cases} 1.1 & , v < 0.1 \\ \frac{0.10}{v^{1.1}} - 0.2 & , 0.1 \leq v \leq 1 \\ -0.1 & , v > 1 \end{cases}$.

Formula (B1) requires T_{pwb} as an input, which can be estimated by using formula (B2).

$$T_{pwb} = 0.376 + 5.79P_a + (0.388 - 0.0465P_a) \times T_a \tag{B2}$$

where P_a is ambient water vapor pressure in kPa.

Formula (B2) requires P_a as an input, which can be estimated by using formula (B3), as applied in program in ISO 7933 [8].

$$P_a = \left(\frac{Rh}{100}\right) \times 0.6105 e^{\left[\frac{17.27 T_a}{T_a + 237.3}\right]} \tag{B3}$$

The second estimation method of T_{nw} is provided by ISO 7243 [9], which is based on the heat balance equation of a wet wick, as shown in formula (B4).

$$4.18 \times v^{0.444}(T_a - T_{nw}) + 10^{-8} \times [(T_{mrt} + 273)^4 - (T_{nw} + 273)^4] - 77.1 \times v^{0.421}[P_{as}(T_{nw}) - Rh \times P_{as}(T_a)] = 0 \tag{B4}$$

where P_{as} is saturated water vapor pressure in kPa, which depends on temperature. Similar to formula B3, we followed formula B5 to estimate P_{as}.

$$P_{as} = 0.6105e^{\left[\frac{17.27T}{T+237.3}\right]} \quad \text{(B5)}$$

Considering that in this study, measurements were conducted under non-static conditions, which results in inaccurate Tg measurement due to the long responding time, we applied formulas B4 and B5 to estimate T_{nw} by using T_{mrt} calculated from 6-directional longwave and shortwave radiation. Bisection method was implemented in R to estimate T_{nw} with an accuracy of 6 decimal places. It is also for the same reason that the T_{nw} output from Kestrel 5400 is not used for HKHI calculation.

Appendix C Field survey details

C.1 Questionnaire used in the field survey

Fig. C1-3 are the questionnaire used in the field survey. The participants were not given a hard copy of the questionnaire, but were asked verbally and responded the same time they experienced the environment. Their responses were taken by using an online survey system. We believe this is a better and more efficient way to have the participants experience the environment rather than reading and then responding to the questions in outdoor environment.

日期：____________ 時間：__________ 天氣概況：____________ 被試編號：____________
Date: _____________ Time: ___________ Weather: ______________ Participant no.: __________

第一部分 行走前的基礎信息收集
Part I: Pre-walk survey for basic information

1. 性別 Biological sex
□男 Male □女 Female

2. 年齡 Age group
□18-25 □26-35 □36-45 □45+

3. 您在過去 2 年是否長期居住在香港? Have you been living in Hong Kong for the last 2 years?
□是 Yes □否 No

4. 您住在這個公共屋邨的年限? How long have you been living in this PHE.
□0 年 0 years. □<2 年 Less than 2 years. □2-5 年 Ranging 2-5 years. □>5 年 Over 5 years.

5. 此前的 30 分鐘您從事的活動是否屬於以下類別?
What types of activities did you engaged in in the previous 30 minutes?
□睡眠 □坐（休息，辦公）□站立 □行走 □運動 □其他_______
□Sleeping □Sitting(Relaxing, working) □Standing □Walking □Exercising □Others_____

6. 您此刻的衣著狀況。What are you wearing?
上衣：□無袖 □短袖 □襯衫 □無
口罩：□有 □無
Upper body: □Non-sleeve □Short-sleeve □Shirts □None
Masks: □Yes □No
褲子：□短褲 □長褲
遮陽帽：□有 □無
Lower body: □Shorts □Trousers
Hat: □Yes □No

Fig. C1 Questionnaire: Part I

第二部分 行走中的熱與環境感知
Part II: Thermal and environmental perception during walking

從您個人的角度出發，請回答下列問題。
Please answer the following questions based on your personal experience.

1. 對於總體環境質量而言您認為此刻，
Concerning the overall environmental quality at this moment, you find it

□-2 差	□-1 較差	□0 適中	□1 較優	□2 優
□-2 Bad	□-1 Slightly bad	□0 Neutral	□1 Slightly Good	□2 Good

2. 對於熱環境而言您認為此刻，
Concerning the thermal environment at this moment, you find it

□-3 冷	□-2 涼爽	□-1 較涼爽	□0 適中	□1 較溫暖	□2 溫暖	□3 炎熱
□-3 Cold	□-2 Cool	□-1 Slightly cool	□0 Neutral	□1 Slightly warm	□2 Warm	□3 Hot

□1 舒適	□2 稍不舒適	□3 不舒適	□4 很不舒適	□5 非常不舒適
□1 Comfortable	□2 Slightly uncomfortable	□3 Uncomfortable	□4 Very uncomfortable	□5 Extremely uncomfortable

□-2 不愉悅	□-1 較不愉悅	□0 適中	□1 較愉悅	□2 愉悅
□-2 Unpleasant	□-1 Slightly unpleasant	□0 Neutral	□1 Slightly pleasant	□2 Pleasant

3. 對於景色的美觀程度您認為，
Concerning the scenic beauty, you find it

□-2 不美观	□-1 較不美观	□0 適中	□1 較美观	□2 美观
□-2 Bad	□-1 Slightly bad	□0 Neutral	□1 Slightly good	□2 Good

4. 對於聲音環境您認為，
Concerning the acoustic environment at this moment, you find it

□-2 吵闹	□-1 較吵闹	□0 適中	□1 較安静	□2 安静
□-2 Noisy	□-1 Slightly noisy	□0 Neutral	□1 Slightly quiet	□2 Quiet

5. 對於光線環境您認為，
Concerning the visual environment at this moment, you find it

□-2 昏暗	□-1 較昏暗	□0 適中	□1 較刺眼	□2 刺眼
□-2 Dim	□-1 Slightly dim	□0 Neutral	□1 Slightly glaring	□2 Glaring

6. 對於空氣質量您認為，
Concerning the air quality at this moment, you find it

□-2 差	□-1 較差	□0 適中	□1 較好	□2 好
□-2 Bad	□-1 Slightly bad	□0 Neutral	□1 Slightly good	□2 Good

7. 對於行走安全感您認為，
Concerning street safety at this moment, you find it

□-2 不安全	□-1 較不安全	□0 適中	□1 較安全	□2 安全
□-2 Unsafe	□-1 Slightly unsafe	□0 Neutral	□1 Slightly safe	□2 Safe

Fig. C2 Questionnaire: Part II

第三部分 行走後調查

Part III: Post-walk survey

1. 您覺得這次行走與您日常的行走經歷是否相似？

Do you think this walk is similar to your daily walking experience?

□很相似 □較相似 □較不相似 □很不相似 □不確定

□Very much □Relatively yes □Relatively not □Very much not □Not sure

如果回答是較*不相似/很不相似*，那麼原因是________

If the answer is *relatively not/very much not*, then the reason is ________.

2. 您認為在屋邨內和屋邨外的行走體驗是否有明顯的區別？

Do you think there is any significant difference in the walking experience inside and outside the estate?

□屋邨內明顯優於屋邨外 □屋邨內較優於屋邨外 □二者相近

□屋邨內較劣於屋邨外 □屋邨內明顯劣於屋邨外 □不確定

3. 您覺得在今天的行走過程中，与热体验相关的感知對整體行走體驗的貢獻程度有多大？

How much do you think thermal perception contributes to the overall walking experience during walking today?

□很大 □大 □少 □很少 □不確定

□Much □Some □Few □Very few □Not sure

如果回答是*少/很少*，那麼什麼因素您認為對行走體驗的貢獻更大________

If the answer is *few/very few*, then what factor(s) do you think contributed the most ________.

4. 您覺得今天行走過程中，綠化對提升您的行走體驗的貢獻有多大？

How much do you think greenery has contributed to improving your walking experience during your walking today?

□很大 □大 □少 □很少 □不確定

□Much □Some □Few □Very few □Not sure

如果回答是*少/很少*，那麼什麼因素您認為對行走體驗的貢獻更大________

If the answer is *few/very few*, then what factor(s) do you think contributed the most ________.

5. 您覺得通過改善今天行走路程中的綠化要素是否能提升您的行走體驗？

Do you think your walking experience can be improved by improving the greenery elements along today's walking route?

□很有可能 □有可能 □很少可能 □很不可能 □不確定

□Very much likely □Likely □Less likely □Unlikely □Not sure

Fig. C3 Questionnaire: Part III

C2 Walking routes and stopping points

As introduced in Section 2.1, three types of public spaces, i.e., open squares, vegetated spaces, and semi-outdoor spaces, are of our interests, and the walking paths are meant to link between these types of spaces. The diversity of the spaces one participant experienced is illustrated in Fig. C4-5, which shows the calculated SVF and GVI of the front view images along two walking trips. More examples of the three types of public spaces as stopping points from each of the five selected PHEs are shown in Fig. C6-8. With similar building typologies, and generic design of the public spaces, they exhibit a striking visual resemblance.

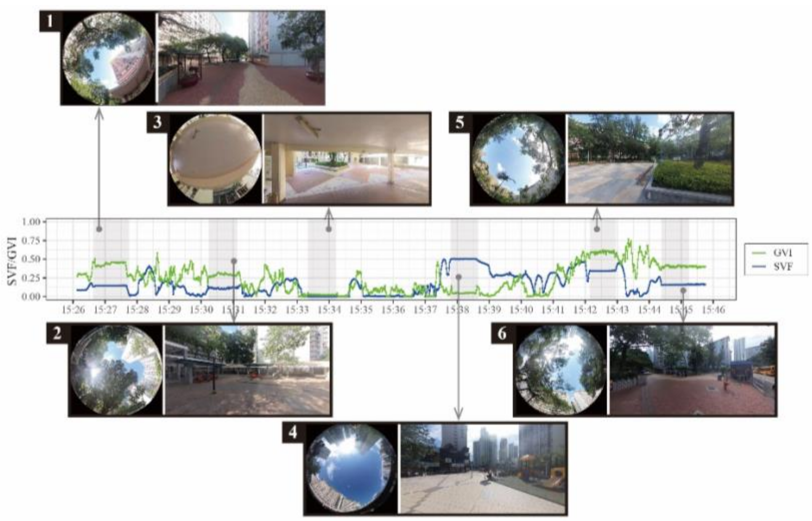

Fig. C4 SVF and GVI variations along the walking trip on Aug. 9, 2023 in Lai Kok and Lai On Estates

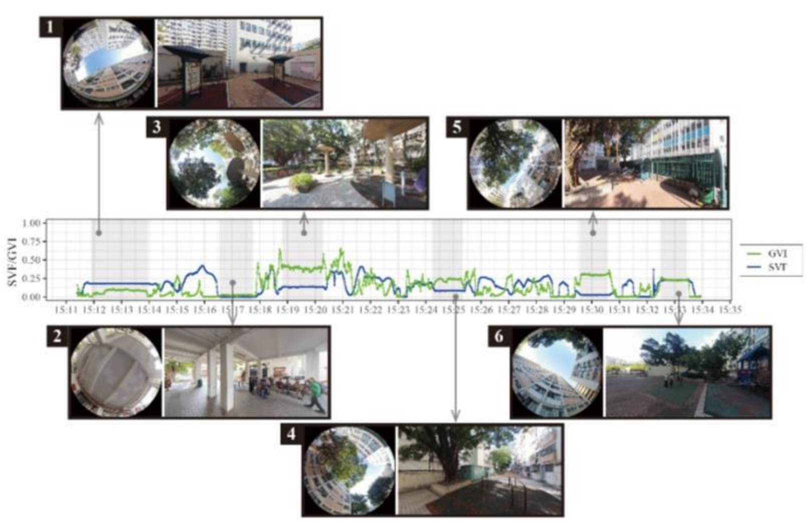

Fig. C5 SVF and GVI variations along the walking trip on Sep. 23, 2023 in Choi Hung Estate

Fig. C6 Sky view and panoramic view of the three types of public spaces as stopping points: open squares

105

106 **Fig. C7** Sky view and panoramic view of the three types of public spaces as stopping points: vegetated spaces

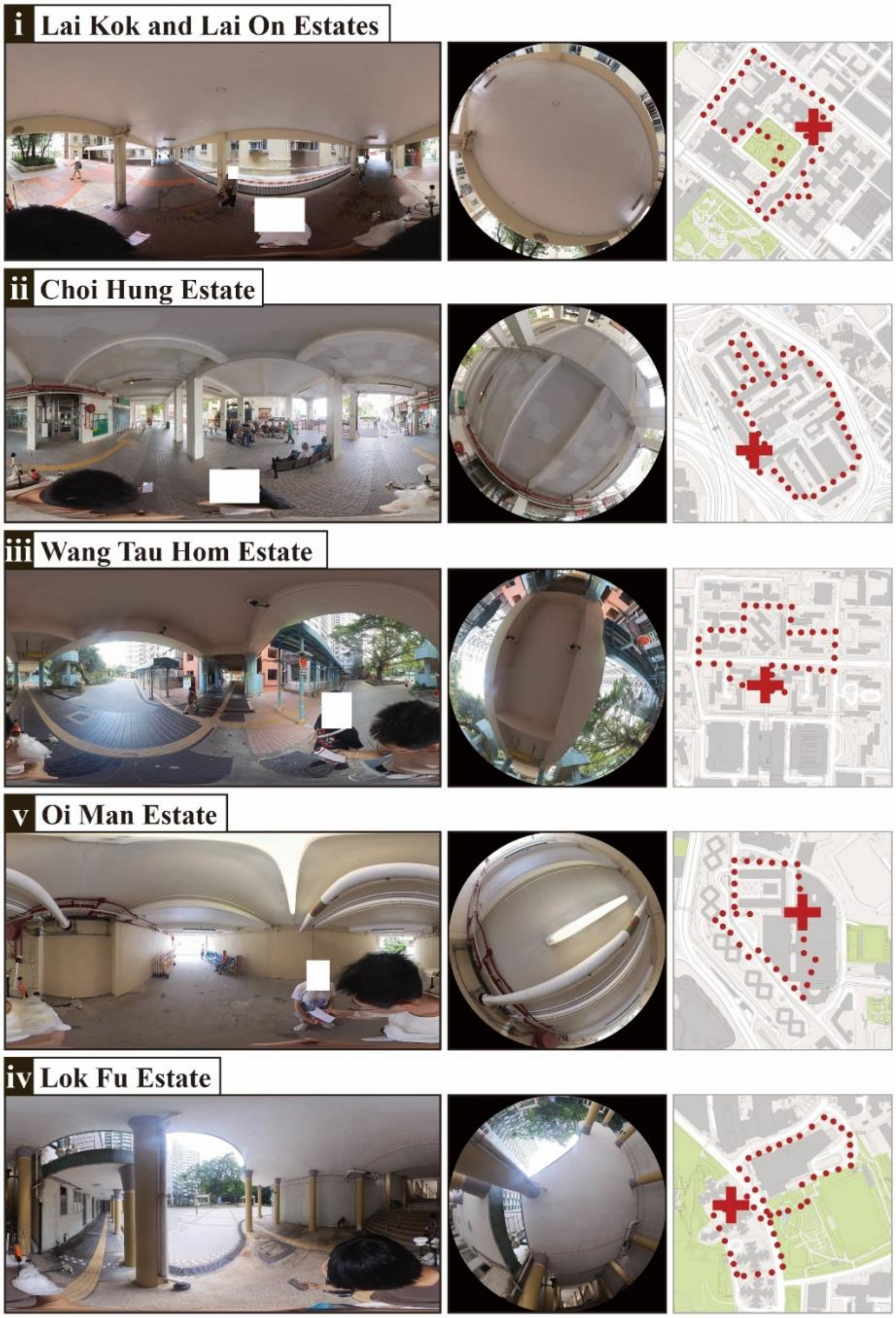

Fig. C8 Sky view and panoramic view of the three types of public spaces as stopping points: semi-outdoor spaces

Appendix D Calculation of built environment characteristics

The panoramic video processing workflow is illustrated in Fig. D1. Video and image processing, and computer vision tasks were accomplished in Python. We used an Insta360 X3 panorama camera to record the simultaneous exposure to the built environment. The video was first exported at a size of 3840×1920 pixel, and we extracted panoramic images by every second. By using a Mask2Former model trained on Cityscapes with Swin-S as backbone [10], semantic segmentation was conducted.

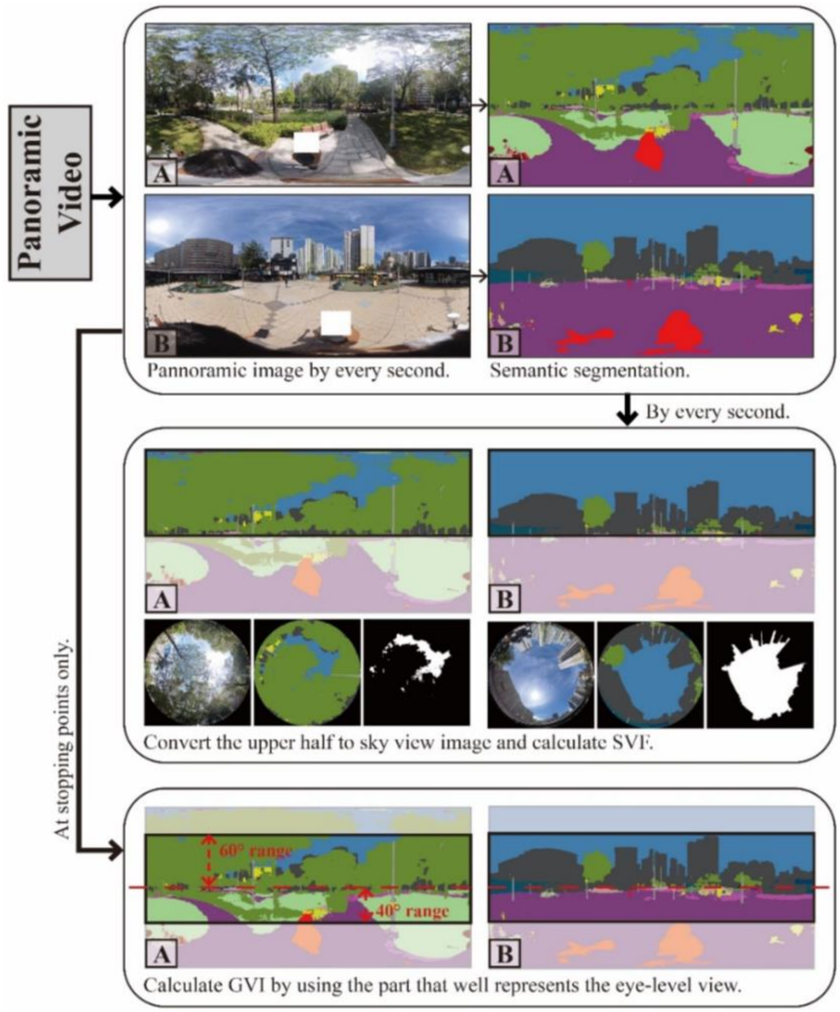

Fig. D1 Panoramic video processing workflow with two examples.

On one hand, following the algorithm of ref. [11], the upper half of the segmentation result is transformed into sky view image, and the areas classified as sky is further used to calculate SVF. We followed the algorithm by Rayman [12,13], as detailed in Rayman manual and by ref.

[14]. As pointed out by ref. [14], the calculation of SVF in Rayman does not weight to include the relation between incoming radiation and zenith angle, which leads to disparities in calculated SVF value compared to other methods. However, as Rayman is widely used to calculate SVF by using fisheye images, we still adopted this calculation method.

On the other hand, the areas classified as vegetation and terrain are used to calculate GVI. It is calculated as the proportion of green pixels out of the total area [15], which describes the visibility of greenery at eye-level [16]. Due to the severe distortion at the top and bottom of the panoramic image, similar to ref. [17], we cropped the panoramic image by selecting the part that well represents the eye-level view, which is the upper 60° range and lower 40° range in our case, as shown in Fig. D1.

Appendix E Results supplementary

E.1 Construction of path analysis and results details

E.1.1 Hypothesis of pathway models

We aim at building pathway models among built environment characteristics, microclimate conditions, physiological parameter, thermal perceptions, and environmental perceptions to reveal their multivariate associations. The following presents the procedures that we formulate the pathway models we examined with the field data.

Model 1 (Fig. E1(a)) evaluates the multivariate association among built environment, microclimate conditions and three aspects of thermal perceptions. Built environment characteristic influences outdoor thermal environment [18], with SVF contributing significantly in summer in public spaces in PHEs [19]. And the thermal environment, quantified by microclimate and thermal comfort indices, further determines subjects' thermal perceptions [20]. In particular, under transient condition, the sensation of thermal environment and its changes determine the comfort perception, and thermal pleasure is likely to be induced when the subject feels "comfortable" as the thermal stress is relieved [21,22]. With the considerations of the affective and hedonic aspects of thermal perception, we construct the three aspects of thermal perceptions in the current form.

Based on Model 1, dTskin is further incorporated as a physiological parameter, considering that Tsk is a crucial indicator of human physiological state and dynamic thermal comfort [22,23].

Based on Model 1, multi-sensory environmental perceptions and overall environmental quality are incorporated. The multi-sensory perceptions are contributors to perceived environment quality of the built environment [24]. Though not an *in-situ* survey, ref. [25] revealed the association between built environment and the perceived environmental quality consisting of safety, aesthetic value etc. We therefore detailed the pathway in this study with field in-situ data in the current form, which incorporates the thermal realm that can only be evaluated on site with thermal stimuli.

Model 4 is constructed by jointly considering all factors stated above. For conciseness, we presented the optimized pathway models in Fig. 5. The detailed results of each model are presented in Section E.1.2.

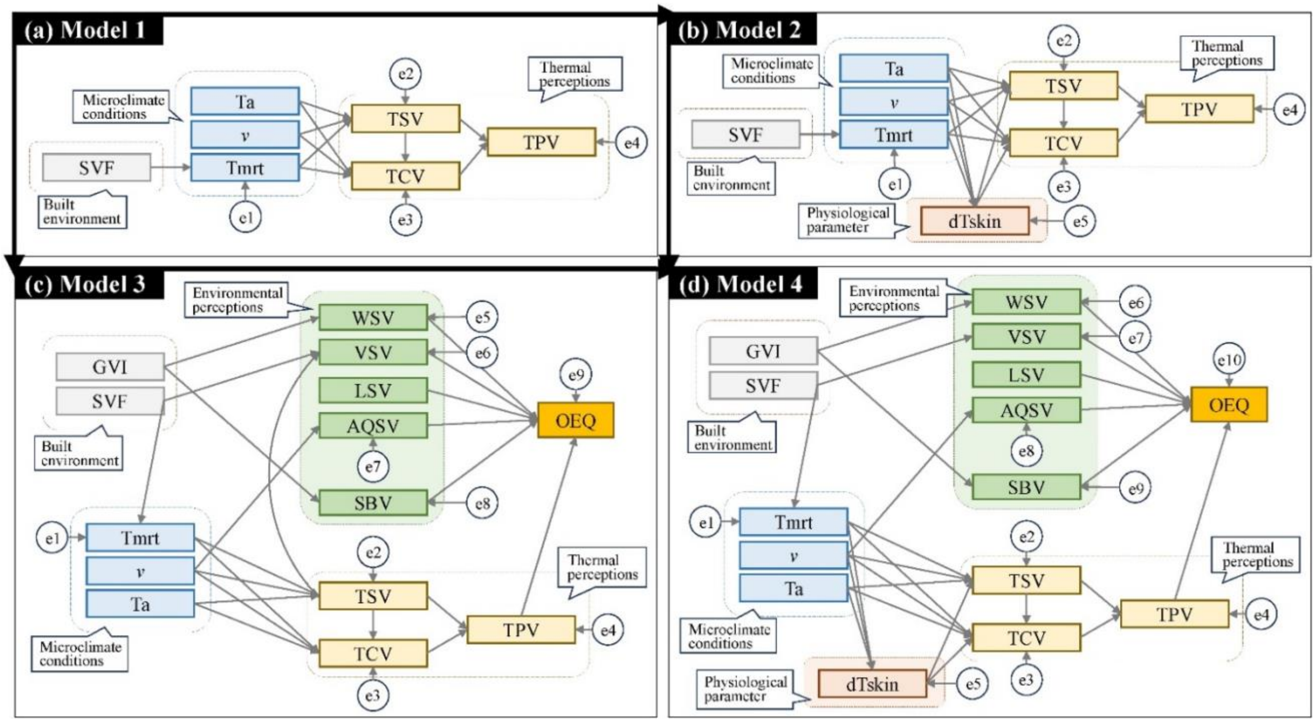

Fig. E1 Hypothesis of pathway models

E.1.2 Detailed model results

Fig. E2 presents the results of Model 1. We tested different combinations of microclimate and thermal comfort indices, and Model 1-3(Fig. E2(e)) is the model with best fit, as quantified by TLI and CLI. Compared to Model 1-1 (Fig. E2(a)), models excluding Ta as an exogeneous variable (Model 1-2, Fig. E2(b-d)) demonstrated better model fits. And the model using mPET (Fig. E2(d)) instead of Tmrt (Fig. E2(b)) demonstrated the best model fit. Therefore, mPET is used in subsequent analyses.

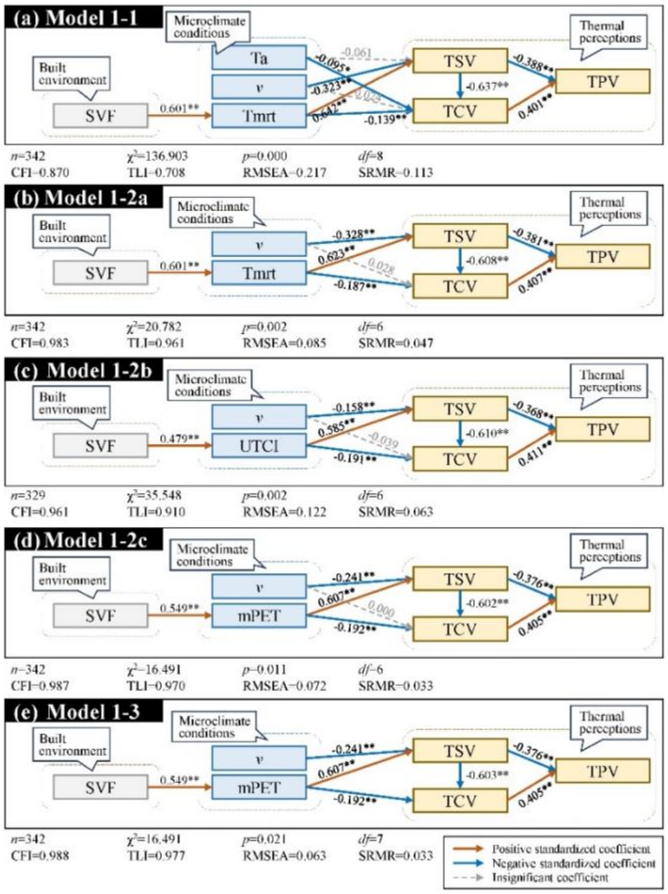

Fig. E2 Pathway models I

By incorporating dTskin as a physiological parameter, the extended model does not demonstrate enhanced model fit, as shown in Fig. E3(b). Nevertheless, dTskin is significantly associated with mPET but not *v*, or any aspects of thermal perceptions.

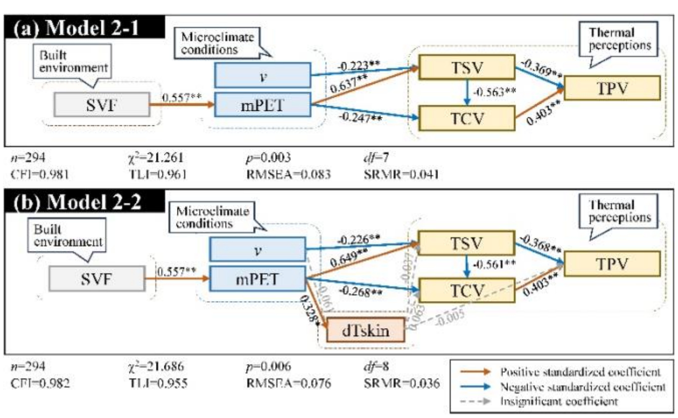

Fig. E3 Pathway models II

Models including multi-sensory environmental perceptions and overall environmental quality are shown in Fig. E4. Poor model fit was obtained when including all multi-sensory perceptions, as shown in Model 3-1 (Fig. E4(a)). Through step-by-step optimization, reasonable model fit (TLI/TFI>0.9) was obtained when only keeping SBV (Fig. E4(f)).

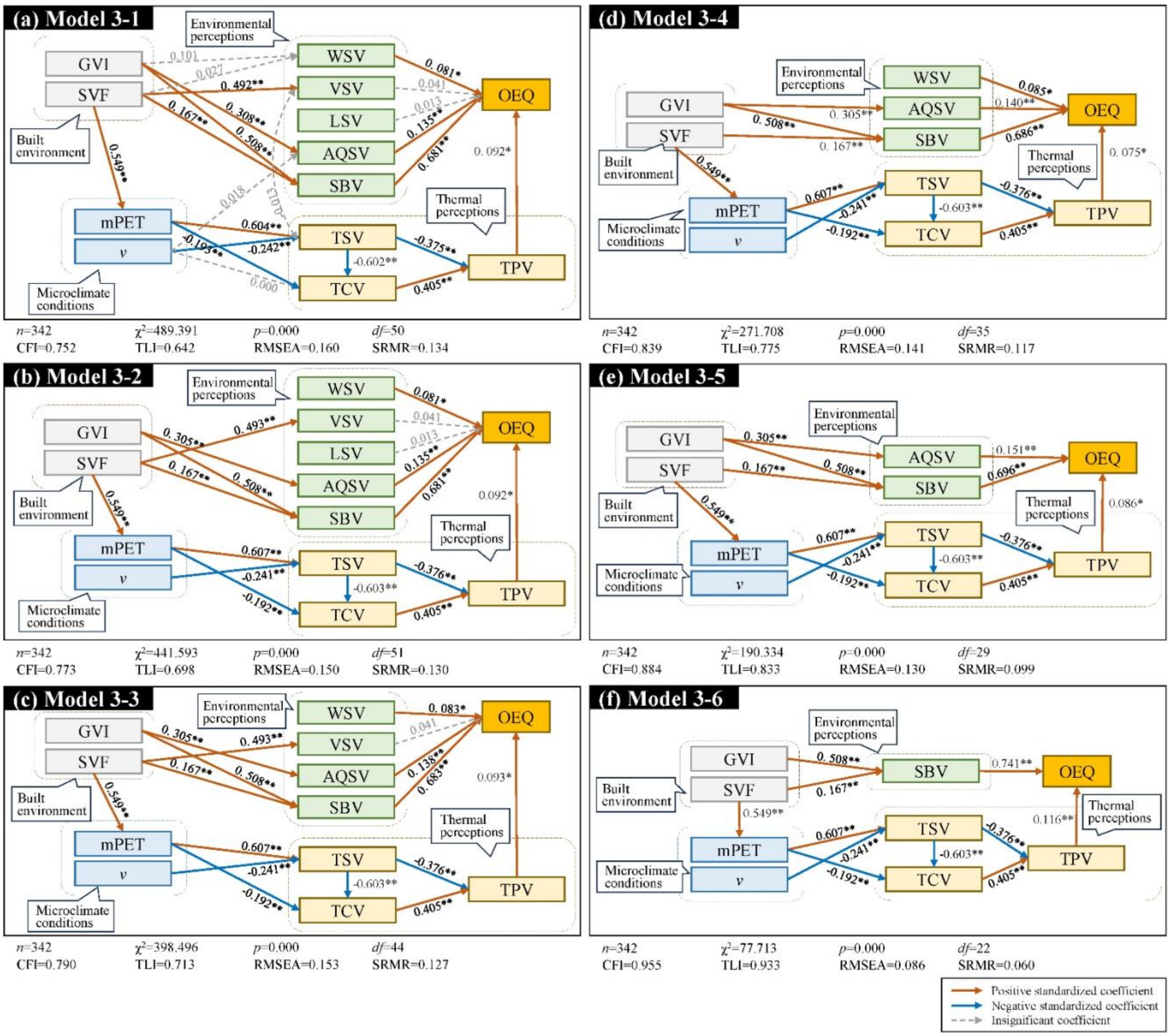

Fig. E4 Pathway models III

The final pathway model is built by incorporating dTskin, as shown in Fig. E5(b), which fits well with the collected data (TLI/CFI>0.9, SRMR<0.08).

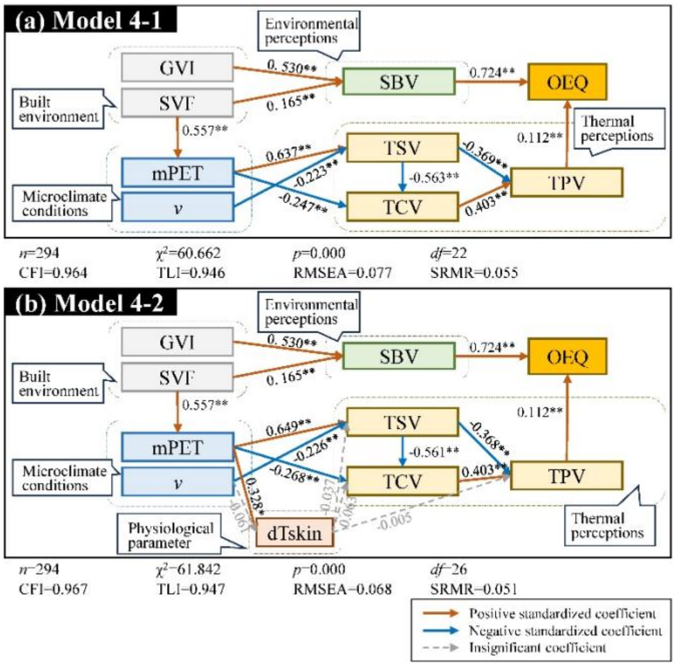

Fig. E5 Pathway models IV

E.2 Calculation of lagged response among variables

The measured variables along two walking trips are shown in Fig. E6 and E7, which explicitly demonstrate the lagged response of Tg and Tsk to radiation, quantified as Tmrt calculated with six-directional radiation. To quantify the lagged response among SVF, Tmrt, Tg and Tsk_m, we applied cross correlation among variables. It calculates the correlation coefficients (ρ) between two time-series variables by shifting one relative to the other over a range of time lags. It allows us to determine both the strength of the correlation and the time lag at which the correlation peaks. Two elements are essential when determining the lagged response, i.e., the direction for data shifting, and the maximum time lag to search for the peak ρ.

When determining the direction for data shifting, we considered the causal relationships and observed responses among variables. Since solar radiation is the cause of changes in Tg and Tsk_m, we therefore shift Tg and Tsk_m relative to Tmrt to find the peak correlation. For the comparison between Tg measured by Kestrel and black table-tennis ball, we observed that the Kestrel sensor exhibits a slower response, which is shown in the examples in Fig. E6 and E7. We therefore shift the Tg measured by Kestrel relative to the Tg measured with black table-tennis ball to determine the lag. For Tsk_m, data show that the response time of Tsk_m is comparable to that of the Tg measured with black table-tennis ball, while Tg measured by Kestrel shows a slower response, and we therefore shift Tg measured with Kestrel to Tsk_m, and search for both directions for Tg measured with black table tennis ball. As for SVF, which quantifies the sky exposure and directly influences radiation, we applied the same searching strategies as Tmrt.

When determining the maximum time lag to search for the peak ρ, we mainly considered the data pattern. The observed faster responses of Tg measured with black table-tennis ball and Tsk_m to radiation is generally within 150s, and that of Tg measured with Kestrel is generally within 300s. Considering the dynamic environment along the walking trips, we consider it inappropriate to apply longer time span.

The corresponding cross correlation results of data presented in Fig. E6 and E7 are presented in Fig. E8 and E9. The red arrows point at where the ρ reaches the maximum, which is identified as the lag time for that sample. When significant correlation does not exist (Fig. E8(h)), or a peak is not found within the search range, it is omitted in the plot presented in Fig. 8.

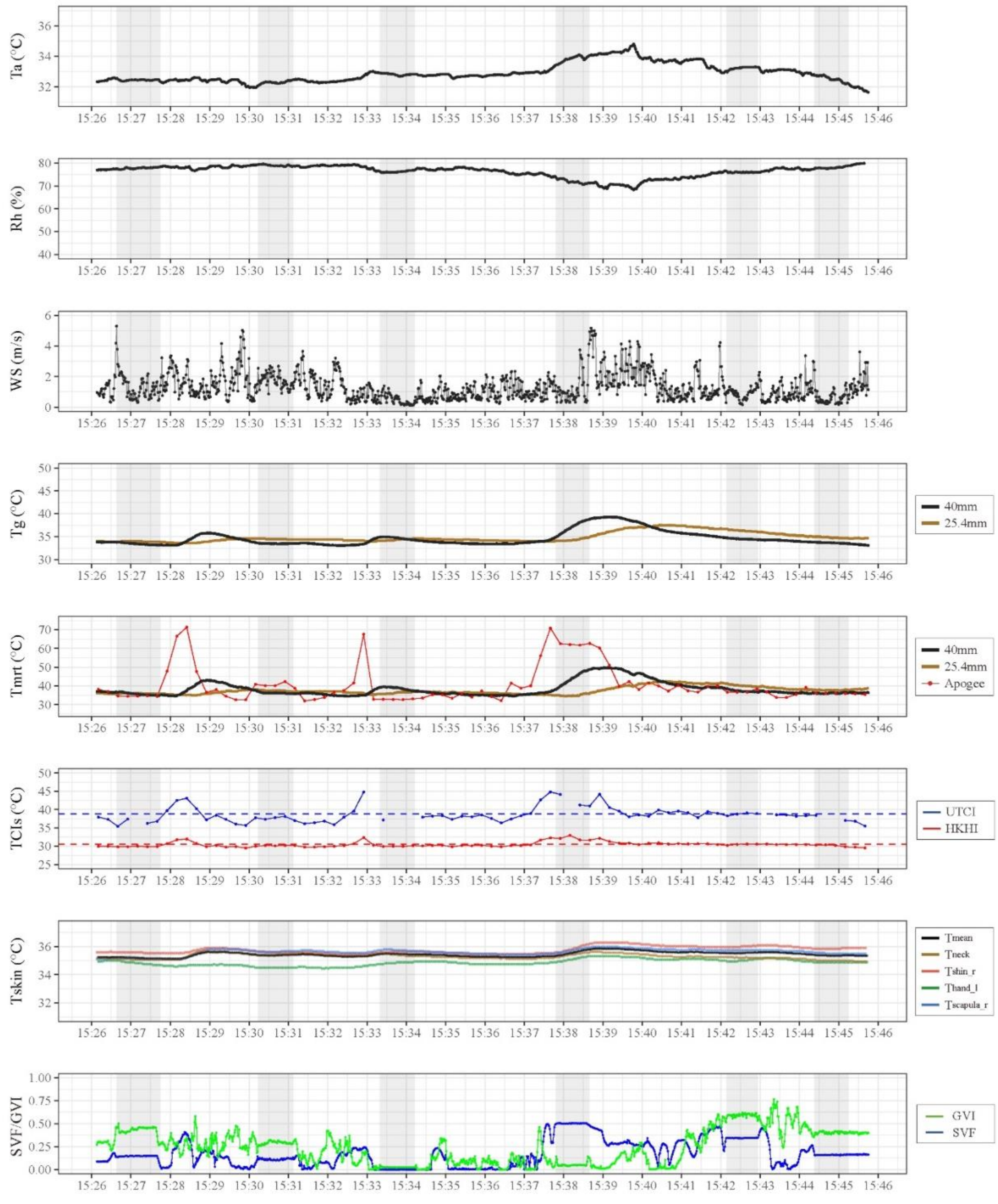

Fig. E6 Walking trip conducted on Aug. 9, 2023 (**Note:** The shaded areas are where the participant was stopped to respond to the questions on thermal and environmental perceptions, and the rest are the walking segments. Missing UTCI values are due to too low *v*. Same below.)

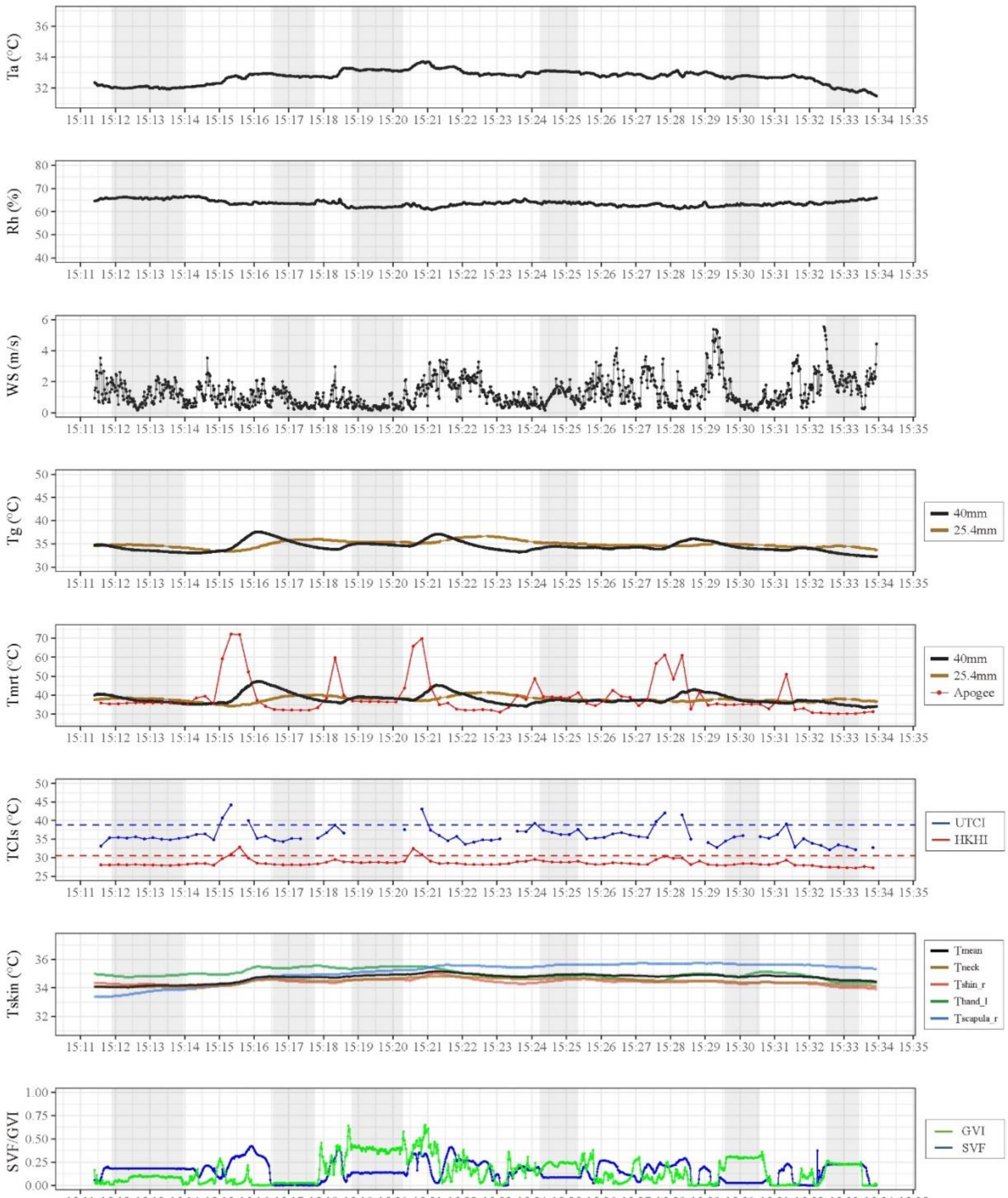

Fig. E7 Walking trip conducted on Sep. 23, 2023

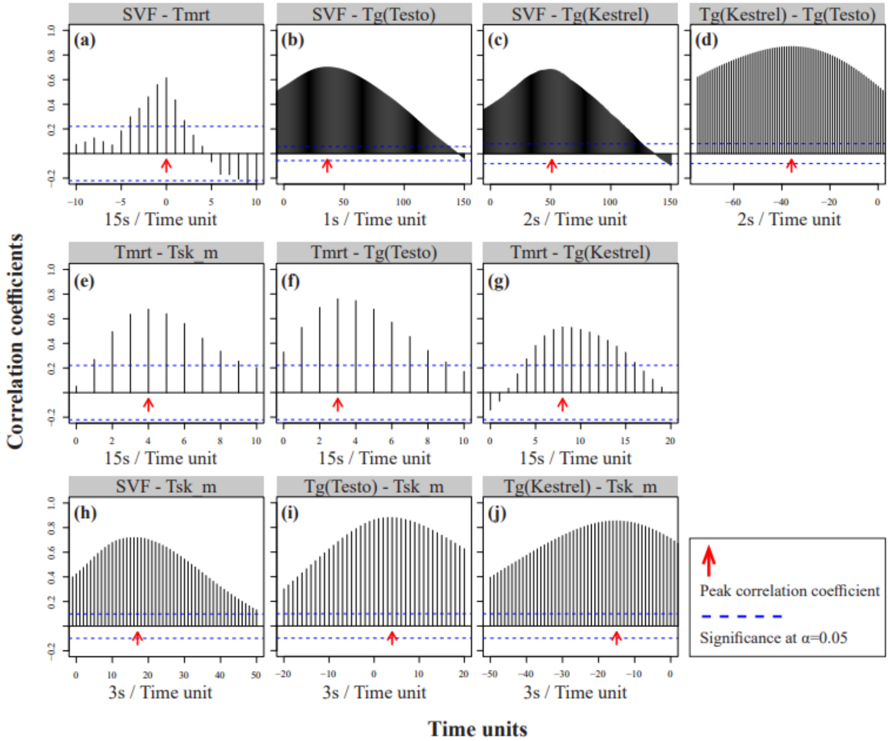

Fig. E8 Cross correlations among variables for data presented in Fig. E6

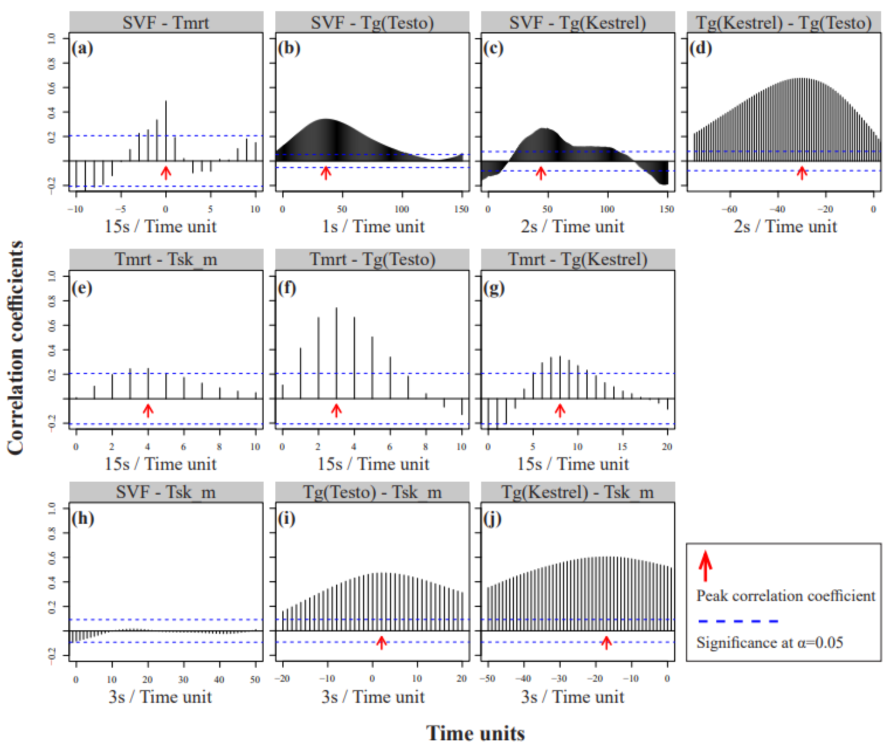

Fig. E9 Cross correlations among variables for data presented in Fig. E7

E.3 Poisson regression result details

Table E1 Poisson regression models between the frequency of self-reported thermal displeasure and microclimate variables

	M1	**M2**	**M3**	**M4**	**M5**	**M6**	**M7**	**M8**	**M9**	**M10**
mPET_sd	-	-	-	-	-	-	-	-	0.39**	0.41**
mPET_mean	-	-	-	-	-	-	-	-	0.07	0.09
UTCI_sd	-	0.73**	-	0.80**	-	0.80**	-	0.82**	-	-
UTCI_mean	-	0.14	-	0.07	-	0.06	-	-	-	-
UTCI_per	-	-0.90	-	-0.09	-	-	-	0.48	-	-
HKHI_sd	2.13**	-	2.38**	-	2.44**	-	2.35**	-	-	-
HKHI_mean	-0.24	-	-0.27	-	-0.07	-	-	-	-	-
HKHI_per	0.80	-	0.99	-	-	-	-0.04	-	-	-
*v*_sd	-0.74	-1.14	-	-	-	-	-	-	-0.80	-
*v*_mean	0.91	1.13	-	-	-	-	-	-	0.76	-
Intercept	5.86	-6.03	6.87	-3.60	1.13	-3.28	-0.81**	-1.08**	-3.43	-4.04
AIC	197.75	199.02	196.72	198.84	195.56	196.85	195.88	197.07	192.52	190.39

Note: *_mean* and *_sd* refer to the mean and SD of microclimate variables along the walking segments. – refers to that the variable is not included when building the model. * and ** refer to significance at 0.05 (two-tailed) and 0.01 (two-tailed) respectively. Same below.

Table E2 Poisson regression models between the frequency of self-reported thermal pleasure and microclimate variables

	M1	**M2**	**M3**	**M4**	**M5**	**M6**	**M7**	**M8**	**M9**	**M10**
mPET_sd	-	-	-	-	-	-	-	-	-0.07	-0.02
mPET_mean	-	-	-	-	-	-	-	-	0.07	0.09
UTCI_sd	-	-0.07	-	0.01	-	0.13	-	-0.02	-	-
UTCI_mean	-	-0.17	-	-0.20*	-	0.05	-	-	-	-
UTCI_per	-	2.35*	-	2.66**	-	-	-	1.05*	-	-
HKHI_sd	-0.01	-	0.23	-	0.33	-	0.01	-	-	-
HKHI_mean	-0.33	-	-0.33*	-	0.10	-	-	-	-	-
HKHI_per	2.21**	-	2.26**	-	-	-	1.13**	-	-	-
*v*_sd	-0.26	-0.27	-	-	-	-	-	-	-0.64	-
*v*_mean	0.62	0.52	-	-	-	-	-	-	0.85*	-
Intercept	10.04*	6.92*	10.53*	8.10*	-1.94	-0.92	1.09**	1.05**	-1.73	-2.08
AIC	254.62	257.74	255.28	256.05	263.71	262.92	257.29	258.35	261.11	261.67

Table E3 Poisson regression models between the frequency of self-reported thermal pleasure and microclimate variables

	M1	**M2**	**M3**	**M4**	**M5**	**M6**	**M7**	**M8**	**M9**	**M10**
mPET_sd	-	-	-	-	-	-	-	-	0.09	0.13
mPET_mean	-	-	-	-	-	-	-	-	0.07	0.08*
UTCI_sd	-	0.23	-	0.30*	-	0.36**	-	0.28*	-	-
UTCI_mean	-	-0.08	-	-0.12	-	0.05	-	-	-	-
UTCI_per	-	1.26	-	1.75*	-	-	-	0.80*	-	-
HKHI_sd	0.78**	-	1.03**	-	1.12**	-	0.87**	-	-	-
HKHI_mean	-0.33*	-	-0.35*	-	0.03	-	-	-	-	-
HKHI_per	1.78**	-	1.89**	-	-	-	0.65*	-	-	-
*v*_sd	-0.42	-0.60	-	-	-	-	-	-	-0.70	-
*v*_mean	0.71*	0.72*	-	-	-	-	-	-	0.82*	-
Intercept	10.22**	3.55	10.96**	5.19	0.29	-0.98	1.08**	0.97**	-1.49	-1.92
AIC	286.93	291.97	289.88	292.51	298.32	296.16	294.27	292.67	290.02	292.00

References

[1] F.A. Obando Vega, A.P. Montoya Ríos, J.A. Osorio Saraz, L.G. Vargas Quiroz, F. Alves Damasceno, Assessment of black globe thermometers employing various sensors and alternative materials, Agricultural and Forest Meteorology 284 (2020) 107891. https://doi.org/10.1016/j.agrformet.2019.107891.

[2] F. d'Ambrosio Alfano, J. Malchaire, B. Palella, G. Riccio, WBGT Index Revisited After 60 Years of Use, The Annals of Occupational Hygiene (2014). https://doi.org/10.1093/annhyg/meu050.

[3] S. Wang, Y. Li, Suitability of acrylic and copper globe thermometers for diurnal outdoor settings, Building and Environment 89 (2015) 279–294. https://doi.org/10.1016/j.buildenv.2015.03.002.

[4] Y.-C. Chen, Thermal indices for human biometeorology based on Python, Sci Rep 13 (2023) 20825. https://doi.org/10.1038/s41598-023-47388-y.

[5] ISO, Ergonomics of the thermal environment. Analytical determination and interpretation of thermal comfort using calculation of the PMV and PPD indices and local thermal comfort criteria, Revision Underway, 2006.

[6] T.E. Bernard, Prediction of Workplace Wet Bulb Global Temperature, Applied Occupational and Environmental Hygiene 14 (1999) 126–134. https://doi.org/10.1080/104732299303296.

[7] A.W. Carter, B.F. Zaitchik, J.M. Gohlke, S. Wang, M.B. Richardson, Methods for Estimating Wet Bulb Globe Temperature From Remote and Low-Cost Data: A Comparative Study in Central Alabama, GeoHealth 4 (2020). https://doi.org/10.1029/2019GH000231.

[8] ISO, Ergonomics of the thermal environment. Analytical determination and interpretation of heat stress using calculation of the predicted heat strain, 2004.

[9] ISO, Ergonomics of the thermal environment. Assessment of heat stress using the WBGT (wet bulb globe temperature) index, 2017.

[10] B. Cheng, I. Misra, A.G. Schwing, A. Kirillov, R. Girdhar, Masked-attention Mask Transformer for Universal Image Segmentation, (2021). https://doi.org/10.48550/ARXIV.2112.01527.

[11] X. Li, C. Ratti, I. Seiferling, Quantifying the shade provision of street trees in urban landscape: A case study in Boston, USA, using Google Street View, Landscape and Urban Planning 169 (2018) 81–91. https://doi.org/10.1016/j.landurbplan.2017.08.011.

[12] A. Matzarakis, F. Rutz, H. Mayer, Modelling radiation fluxes in simple and complex environments—application of the RayMan model, Int J Biometeorol 51 (2007) 323–334. https://doi.org/10.1007/s00484-006-0061-8.

[13] A. Matzarakis, F. Rutz, H. Mayer, Modelling radiation fluxes in simple and complex environments: basics of the RayMan model, Int J Biometeorol 54 (2010) 131–139. https://doi.org/10.1007/s00484-009-0261-0.

[14] M. Hämmerle, T. Gál, J. Unger, A. Matzarakis, Comparison of models calculating the sky view factor used for urban climate investigations, Theor Appl Climatol 105 (2011) 521–527. https://doi.org/10.1007/s00704-011-0402-3.

[15] X. Li, C. Zhang, W. Li, R. Ricard, Q. Meng, W. Zhang, Assessing street-level urban greenery using Google Street View and a modified green view index, Urban Forestry & Urban Greening 14 (2015) 675–685. https://doi.org/10.1016/j.ufug.2015.06.006.

[16] J. Yang, L. Zhao, J. Mcbride, P. Gong, Can you see green? Assessing the visibility of urban forests in cities, Landscape and Urban Planning 91 (2009) 97–104. https://doi.org/10.1016/j.landurbplan.2008.12.004.

[17] D. Ki, S. Lee, Analyzing the effects of Green View Index of neighborhood streets on walking time using Google Street View and deep learning, Landscape and Urban Planning 205 (2021) 103920. https://doi.org/10.1016/j.landurbplan.2020.103920.

[18] D. Lai, W. Liu, T. Gan, K. Liu, Q. Chen, A review of mitigating strategies to improve the thermal environment and thermal comfort in urban outdoor spaces, Science of The Total Environment 661 (2019) 337–353. https://doi.org/10.1016/j.scitotenv.2019.01.062.

[19] Y. Li, W. Ouyang, S. Yin, Z. Tan, C. Ren, Microclimate and its influencing factors in residential public spaces during heat waves: An empirical study in Hong Kong, Building and Environment (2023) 110225. https://doi.org/10.1016/j.buildenv.2023.110225.

[20] D. Lai, Z. Lian, W. Liu, C. Guo, W. Liu, K. Liu, Q. Chen, A comprehensive review of thermal comfort studies in urban open spaces, Science of The Total Environment 742 (2020) 140092. https://doi.org/10.1016/j.scitotenv.2020.140092.

[21] R. de Dear, Revisiting an old hypothesis of human thermal perception: alliesthesia, Building Research & Information 39 (2011) 108–117. https://doi.org/10.1080/09613218.2011.552269.

[22] M. Vellei, R. De Dear, C. Inard, O. Jay, Dynamic thermal perception: A review and agenda for future experimental research, Building and Environment 205 (2021) 108269. https://doi.org/10.1016/j.buildenv.2021.108269.

[23] J.K. Vanos, J.S. Warland, T.J. Gillespie, N.A. Kenny, Review of the physiology of human thermal comfort while exercising in urban landscapes and implications for bioclimatic design, Int J Biometeorol 54 (2010) 319–334. https://doi.org/10.1007/s00484-010-0301-9.

[24] C. Spence, Senses of place: architectural design for the multisensory mind, Cogn. Research 5 (2020) 46. https://doi.org/10.1186/s41235-020-00243-4.

[25] L. Luo, B. Jiang, From oppressiveness to stress: A development of Stress Reduction Theory in the context of contemporary high-density city, Journal of Environmental Psychology 84 (2022) 101883. https://doi.org/10.1016/j.jenvp.2022.101883.